Edith Cowan University

Research Online

Research outputs 2012

1-1-2012

GaAs based long-wavelength microring resonator optical switches utilising bias assisted carrier-injection induced refractive index change

S Ravindran

A Datta

Kamal Alameh
Edith Cowan University

Yong Tak Lee

Follow this and additional works at: https://ro.ecu.edu.au/ecuworks2012

Part of the Engineering Commons

10.1364/OE.20.015610

This is an Author's Accepted Manuscript of: Ravindran, S., Datta, A., Alameh, K. , & Lee, Y. (2012). GaAs based long-wavelength microring resonator optical switches utilising bias assisted carrier-injection induced refractive index change. Optics Express, 20(14), 15610-15627. Available here
This Journal Article is posted at Research Online.
https://ro.ecu.edu.au/ecuworks2012/254

GaAs based *long-wavelength* microring resonator optical switches utilising bias assisted carrier-injection induced refractive index change

Sooraj Ravindran,[1] **Arnab Datta,**[2] **Kamal Alameh,**[2,4] **and Yong Tak Lee** [1,2,3,*]

[1] *School of Information and Communications, Gwangju Institute of Science and Technology (GIST), 1, Oryong-dong, Buk-gu, Gwangju, 500-712, South Korea*
[2] *Dept. of Nano-bio materials and Electronics, GIST, 500-712, South Korea*
[3] *School of Photonics and Applied Physics, GIST, 500-712, South Korea*
[4] *Centre of Excellence for MicroPhotonic Systems, Electron Science Research Institute, Edith Cowan University, WA, Australia*

[*] *ytlee@gist.ac.kr*

Abstract: We propose and analyse a GaAs-based optical switch having a ring resonator configuration which can switch optical telecommunication signals over the 1300 nm and 1500 nm bands, using bias assisted carrier injection as the switching mechanism. The switching is achieved through variation in the refractive index of the ring resonator produced by changing the injected carrier density through the application of bias voltage. Detail analysis of the switching characteristics reveals that the amount of switching depends on the refractive index change, which indeed is a strong function of injected carrier density and applied bias voltage. An isolation of 25 dB can be achieved during the ON state, while more than 40 dB isolation is realised during the OFF state. More importantly, our analysis shows that the proposed GaAs-based switch can operate over the 1300 nm and 1500 nm optical telecommunication bands, that are much farther from the bandgap of the GaAs material, without the need for *"conventional"* Indium based ternary and quaternary semiconductor materials. It therefore extends the usable wavelength of GaAs based optoelectronic devices. Furthermore, we have presented detail calculations to quantify power-delay metric of the proposed device. The proposed optical switch maintains a smaller footprint as when compared to Mach-Zehnder Interferometer or Directional Coupler based switches therefore, making it suitable for large scale integration and implementing next generation optical interconnects, optical communication and computing.

© 2012 Optical Society of America

OCIS codes: (060.1810) Buffers, couplers, routers, switches, and multiplexers; (130.0250) Optoelectronics; (130.4815) Optical switching devices; (230.3120) Integrated optics devices.

References and links

1. K. Shimomura and S. Arai, "Semiconductor waveguide optical switches and modulators," Fiber Int. Opt. **13**, 65–100 (1992).

#157025 - $15.00 USD Received 25 Oct 2011; revised 8 Apr 2012; accepted 12 Apr 2012; published 26 Jun 2012

2. R. C. Alferness, "Waveguide electrooptic modulators," IEEE Trans. Microw. Theory Tech. **30**, 1121–1137 (1982).
3. T. Tamir, *Integrated Optics* (Springer-Verlang, 1979).
4. G. I. Papadimitriou, C. Papazoglou, A. S. Pomportsis, and I. Tutorial, "Optical switching: switch fabrics, techniques, and architectures," J. Lightwave Technol. **21**, 384–405 (2003).
5. P.K.Basu, *Theory of Optical Processes in Semiconductors-Bulk and Microstructures,* (Oxford Science Publications, 1997).
6. O. Mikami and H. Nakagome, "Waveguided optical switch in InGaAs/InP using free-carrier plasma dispersion," Electron. Lett. **20**, 228–229 (1984).
7. N. Dagli, "Wide-bandwidth lasers and modulators for RF photonics," IEEE Trans. Microw. Theory Tech. **47**, 1151–1171 (1999).
8. G. Li and P. Yu, "Optical intensity modulators for digital and analog applications," J. Lightwave Technol. **21**, 2010–2030 (2003).
9. S. Ng, S. Abdalla, P. Barrios, A. Delage, S. Janz, R. McKinnon, and B. Syrett, "Bend loss attenuator by carrier injection in InGaAsP/InP," Electron. Lett. **41**, 1348–1350 (2005).
10. F. Ito and T. Tanifuji, "Carrier-injection-type optical switch in GaAs with a 1.06-1.55 μm wavelength range," Appl. Phys. Lett. **54**, 134–136 (1989).
11. S. Abdalla, S. Ng, P. Barrios, D. Celo, A. Delage, S. El-Mougy, I. Golub, J.-J. He, S. Janz, R. McKinnon, P. Poole, S. Raymond, T. Smy, and B. Syrett, "Carrier injection-based digital optical switch with reconfigurable output waveguide arms," IEEE Photon. Technol. Lett. **16**, 1038–1040 (2004).
12. G. Muller, L. Stoll, G. Schulte-Roth, and U. Wolff, "Low current plasma effect optical switch on InP," Electron. Lett. **26**, 115–117 (1990).
13. H. Simos, A. Bogris, A. Raptis, N. Raptis, and D. Syvridis, "Dynamic properties of a WDM switching module based on active microring resonators," IEEE Photon. Technol. Lett. **22**, 206–208, (2010)
14. Chao Li, Linjie Zhou, and Andrew W. Poon, "Silicon microring carrier-injection-based modulators/switches with tunable extinction ratios and OR-logic switching by using waveguide cross-coupling," Opt. Express **15**, 5069–5076 (2007).
15. T.A. Ibrahim, W. Cao, Y. Kim, J. Li, J. Goldhar, P.-T. Ho, and C.H. Lee, "All-optical switching in a laterally coupled microring resonator by carrier injection," IEEE Photon. Technol. Lett. **15**, 36–38, (2003)
16. B. Little, S. Chu, H. Haus, J. Foresi, and J.-P. Laine, "Microring resonator channel dropping filters," J. Lightwave Technol. **15**, 998–1005 (1997).
17. D. G. Rabus, M. Hamacher, and H. Heidrich, "Resonance frequency tuning of a double ring resonator in GaInAsP/InP: experiment and simulation," Jpn. J. Appl. Phys. **41**, 1186–1189 (2002).
18. S. Manipatruni, L. Chen, and M. Lipson, "Ultra high bandwidth WDM using silicon microring modulators," Opt. Express **18**, 16858–16867 (2010).
19. T. Sadagopan, S. Choi, S. J. Choi, K. Djordjev, and P. Dapkus, "Carrier-induced refractive index changes in InP-based circular microresonators for low-voltage high-speed modulation," IEEE Photon. Technol. Lett. **17**, 414–416 (2005).
20. T. Wood, "Multiple quantum well (MQW) waveguide modulators," J. Lightwave Technol. **6**, 743–757 (1988).
21. S. J. Emelett and R. Soref, "Design and simulation of silicon microring optical routing switches," J. Lightwave Technol. **23**, 1800–1807, (2005).
22. S. Ravindran, K. Alameh, and Y.-T. Lee, "Design and analysis of electroabsorptive quantum well based double ring resonators for wavelength switching applications," Opt. Quantum Electron. **41**, 635–644 (2009).
23. K. Djordjev, S.-J. Choi, S.-J. Choi, and P. Dapkus, "Active semiconductor microdisk devices," J. Lightwave Technol. **20**, 105–113 (2002).
24. B. Little, H. Haus, J. Foresi, L. Kimerling, E. Ippen, and D. Ripin, "Wavelength switching and routing using absorption and resonance," IEEE Photon. Technol. Lett. **10**, 816–818 (1998).
25. K. Djordjev, S.-J. Choi, S.-J. Choi, and R. Dapkus, "Microdisk tunable resonant filters and switches," IEEE Photon. Technol. Lett. **14**, 828–830 (2002).
26. J. Piprek, *Semiconductor Optoelectronic Devices-Introduction to Physics and Simulation* (Academic Press, 2003).
27. J. Baliga, *Fundamentals of Power Semiconductor Devices* (Springer Science, 2008).
28. J.-P. Weber, "Optimization of the carrier-induced effective index change in InGaAsP waveguides-application to tunable bragg filters," IEEE J. Quantum Electron. **30**, 1801–1816 (1994).
29. C. Glingener, D. Schulz, and E. Voges, "Modeling of optical waveguide modulators on III-V semiconductors," IEEE J. Quantum Electron. **31**, 101–112 (1995).
30. K.J.Ebeling, *Integrated Optoelectronics* (Springer-Verlang, 1992).
31. J. Faist and F.-K. Reinhart, "Phase modulation in GaAs/AlGaAs double heterostructures. I. theory," J. Appl. Phys. **67**, 6998–7005 (1990).
32. B. Bennett and R. Soref, "Electrorefraction and electroabsorption in InP, GaAs, GaSb, InAs, and InSb," IEEE J. Quantum Electron. **23**, 2159–2166 (1987).
33. J. G. Mendoza-Alvarez, R. H. Yan, and L. A. Coldren, "Contribution of the band-filling effect to the effective refractive-index change in double-heterostructure GaAs/AlGaAs phase modulators," J. Appl. Phys. **62**, 4548–

#157025 - $15.00 USD Received 25 Oct 2011; revised 8 Apr 2012; accepted 12 Apr 2012; published 26 Jun 2012
(C) 2012 OSA

4553 (1987).
34. B. Bennett, R. Soref, and J. Del Alamo, "Carrier-induced change in refractive index of InP, GaAs and InGaAsP," IEEE J. Quantum Electron. of **26**, 113–122 (1990).
35. J. G. Mendoza-Alvarez, F. D. Nunes, and N. B. Patel, "Refractive index dependence on free carriers for GaAs," J. Appl. Phys. **51**, 4365–4367 (1980).
36. S. M. Sze and K. K. Ng, *Physics of Semiconductor Devices* (John Wiley and Sons, 2007).
37. K. Loi, L. Shen, H. Wieder, and W. Chang, "Electroabsorption waveguide modulators at 1.3 μm fabricated on GaAs substrates," IEEE Photon. Technol. Lett. **9**, 1229–1231 (1997).
38. L. Shen, H. Wieder, and W. Chang, "Electroabsorption modulation at 1.3 μm on GaAs substrates using a step-graded low temperature grown InAlAs buffer," IEEE Photon. Technol. Lett. **8**, 352–354 (1996).
39. S. M. Lord, B. Pezeshki, and J. S. Harris, "Electroabsorption modulators operating at 1.3 μm on GaAs substrates," Opt. Quantum Electron. **25**, S953–S964 (1993).

1. Introduction

Optical switches that can switch optical signals from one channel to another in response to a control signal constitute an important functional block in optical communication systems, optical signal processing and optical computing [1]. Optical switches based on refractive index (RI) changes can be realized using various modulation mechanisms, such as electro-optic (EO) [2], acousto-optic [3], magneto-optic [3], thermo-optic (TO) [4], electro-absorption (EA) [5–7], and bias assisted carrier-injection (CI) effects [5, 6]. Note that, guided-wave optical switches are usually made of Lithium-Niobate ($LiNbO_3$) which uses EO effect as the primary switching mechanism. However, $LiNbO_3$ is not a compatible material for integration with conventional III-V semiconductor platforms. On the other hand, optical switches based on III-V semiconductor materials offer an attractive alternative since they allow monolithic integration with other III-V devices such as lasers, amplifiers and photodetectors.

Optical switches based on III-V semiconductor materials enable other switching mechanisms (such as EA and CI) in addition to the EO effect, thus allowing proper signal channeling in the switches through custom tailoring the RI of the material, and hence the optical confinement. Each of the above mentioned switching mechanisms demand different criteria for optical switch design. For example, the EA effect requires the material to have a bandgap close to the photon energy of the optical signal to be switched, and is polarisation sensitive [7]. This imposes severe restrictions on the choice of semiconductor materials that can be used for the switch as well as the operational wavelength at which the switch can function. The EO effect is relatively weak in III-V semiconductors, polarisation sensitive, and demands a long device length of the order of millimeter to attain practical optical switching [8]. TO effect based switches suffer from high driving power requirement, and can produce only low RI change [4]. Switches based on CI effect, on the other hand, are more attractive over EO, TO and EA based switches due to their ability to produce large refractive index changes [9–11]. In addition, CI switches are polarisation independent [9] and have been implemented using Mach-Zehnder interferometer (MZI) and Directional Coupler (DC) configurations [10]. Despite their simplicity in operation, CI switches (MZI or DC type) have large device foot-prints, and hence, they are impractical for use in large-scale integrated systems [11, 12].

A potential switch configuration that can replace colossal MZI or DC switch is the micro-ring resonator [16]. Ring resonator based devices have gained significant attention due to their small dimensions (few μm $\times$ μm), which enables denser integration of devices onto optoelectronic integrated chips. A micro-ring resonator device is typically implemented in the form of a ring that is made closely coupled to a waveguide. Optical signals launched in the waveguide couple to the ring, and the ring can support only those signals whose wavelengths are an integer multiple of the ring circumference (called resonant wavelengths). Such optical signals can be extracted by placing a second waveguide adjacent to the ring. In fact, ring resonator devices can function as tunable filters [17], modulators [18, 19] and lasers, and hence, they have the

#157025 - $15.00 USD Received 25 Oct 2011; revised 8 Apr 2012; accepted 12 Apr 2012; published 26 Jun 2012
(C) 2012 OSA

potential to be adopted for optical switching applications.

In this paper, we propose and analyse a GaAs based optical switch that combines the advantages of ring resonators for wavelength selection and electrical bias assisted CI mechanism for injected carriers to alter the RI of the ring, to modify the resonant condition of the ring for switching the resonant optical signal between the two ports.

In principle, carriers are injected by forward biasing a ring resonator structure incorporated as a p-i-n diode heterostructure. The injected carriers alter the refractive index of the ring, thus modifies the resonant condition of the ring for switching the resonant optical signal between the two ports.

The primary advantage of the proposed switch is that the switch size is much smaller than that of an MZI or DC based optical switch, making it ideal for large-scale integration. Also, since the switch is laid on p-i-n semiconducting diode rather than quantum wells [13], the fabrication is much simpler compared to that of EA switches. The latter requires quantum well formation, and hence, precise well width adjustment and lattice matching [20]. Further, in contrast to EA switches, the bandgap of the material need not be close to the optical signal wavelength; thus giving a noticeable freedom to choose between the material and operating wavelength of the switch, especially for longer wavelengths where the available material choices (Indium based [39]) are limited, expensive, and are of inferior quality. The proposed GaAs ring-resonator device can therefore successfully enable switching of long wavelengths such as 1550 nm and 1300 nm, without the usage of any InP based materials. Also, polarisation independent switching is expected since the CI mechanism used for switching is inherently polarisation insensitive. Furthermore, as the signal energy is much smaller than the GaAs bandgap, signal losses due to residual absorption of the guiding material is the least. Above all, unlike silicon based switches [14], monolithic integration with other compund semiconductor devices is readily possible.

The paper is organized as follows: Section 2 provides the structural detail and operating principle of the proposed switch. Injected carrier of the device as a function of applied bias is obtained after solving the diode Drift-Diffusion equations, and are presented in Section 3. Section 3 also elaborates the calculation of index change for a given carrier density. Optical switching characteristics of the proposed device are presented in Section 3.3. A detail electrical switching performance of the device is assessed thereafter in Section 4, followed by conclusion.

2. Device structure and principle of operation

Figure 1 shows the perspective view of the proposed device which can switch optical signals between two output ports (D port and T port). The device consists of two identical rings, each having a radius R, which are coupled and placed in close proximity between two parallel waveguides. For the two ring configuration shown in Fig. 1, the dropped signals and transmitted signals propagate through different waveguides, thereby aiding the interconnection of several such ring devices in addition to providing more design freedom [21].

The cross section of the device has a p-i-n double heterojunction diode structure, whose intrinsic region (i) is made of undoped GaAs having a smaller bandgap (1.424 eV, larger index) sandwiched between p- and n-doped AlGaAs regions having larger bandgap (1.80 eV, smaller index). The i region thus acts as the core for light propagation, while the p and n regions serve as the cladding. The two p electrodes are deposited on the top of the rings, while a single n electrode is deposited beneath the substrate thereby enabling carrier injection through a forward bias (a positive voltage applied onto the p electrodes). Compared to optical pumping [15], electrical injection scheme is more practical. The whole structure is grown on a GaAs substrate. Deep vertical etching assists photon confinement along lateral direction, while the index contrast between p and n AlGaAs cladding and GaAs core confines the light in vertical direction.

#157025 - $15.00 USD Received 25 Oct 2011; revised 8 Apr 2012; accepted 12 Apr 2012; published 26 Jun 2012
(C) 2012 OSA

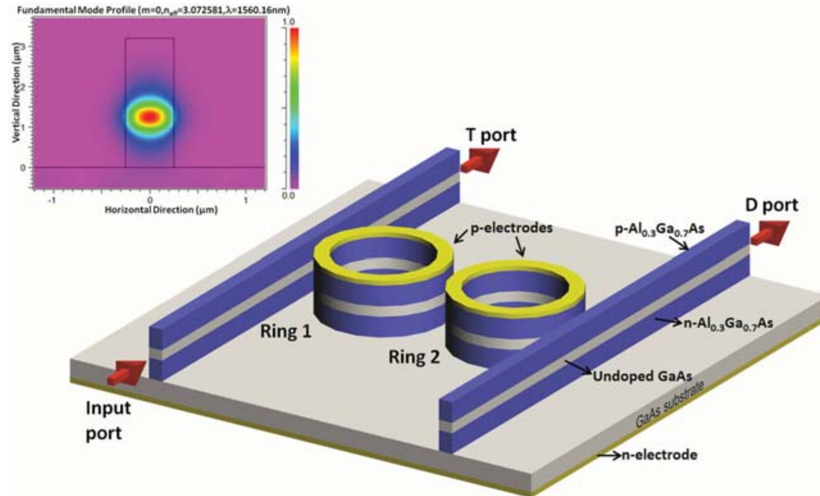

Fig. 1. Perspective view of the proposed switch. The intrinsic region of the rings and of the straight waveguides lies in the same plane. (inset) BPM simulations showing the single mode operation. The red contour denotes the maximum modal confinement.

BeamPROP simulation illustrates tight single mode power confinement for the specified ring p-i-n device (see Fig. 1 (inset)). Note that, both p-and n- AlGaAs cladding thickness are taken around 1.5 μm, which invariably reduces optical mode coupling with the metal electrodes.

From a series of signals launched at the input port, only those special signals whose wavelengths satisfy the condition $m\lambda_R = 2\pi Rn$ (i.e resonance condition, λ_R: resonant wavelength) couple to the rings and appears at the Drop (D) port, while the remaining signals bypass the ring and appear at the Transmit (T) port. Here R is the radius of the ring, n is the core index of ring, and m is an integer. Apart from satisfying the resonant condition, the photon energy corresponding to λ_R has to be smaller than the bandgap of the core material (E_{core}) i.e, $E_{\lambda_R} = hc/\lambda_R \ll E_{core}$, so that λ_R can be collected at D port without undergoing any absorption losses.

It can be shown that in the case of two ring resonators coupled as shown in Fig. 1, the normalised power at the T port (P_T) and D port (P_D) can be expressed as [22]

$$P_T = \left| \frac{\tau_a \exp\left(\frac{2j\omega L}{c}n - \alpha L\right) - \tau_b(1+\tau_a^2)\exp\left(\frac{j\omega L}{c}n - \frac{L}{2}\alpha\right) + \tau_a}{1 - 2\tau_a\tau_b \exp\left(\frac{j\omega L}{c}n - \frac{L}{2}\alpha\right) + \tau_a^2 \exp\left(\frac{2j\omega L}{c}n - \alpha L\right)} \right|^2 \quad (1)$$

and

$$P_D = \left| \frac{j\kappa_a^2\kappa_b \exp\left(\frac{j\omega L}{c}n - \frac{L}{2}\alpha\right)}{1 - 2\tau_a\tau_b \exp\left(\frac{j\omega L}{c}n - \frac{L}{2}\alpha\right) + \tau_a^2 \exp\left(\frac{2j\omega L}{c}n - \alpha L\right)} \right|^2 \quad (2)$$

respectively. Here, α is the absorption coefficient due to losses in the light guide, $L = 2\pi R$ is the circumference of the ring, and $\omega = 2\pi c/\lambda$ represents the angular frequency of the circulating light. τ_a and κ_a represents the transmission and coupling coefficients, respectively at the coupling regions where the ring is in close proximity with the waveguide, whereas τ_b and κ_b represents the transmission and coupling coefficient, respectively, at the region where the rings

#157025 - $15.00 USD Received 25 Oct 2011; revised 8 Apr 2012; accepted 12 Apr 2012; published 26 Jun 2012
(C) 2012 OSA

are coupled to one another. We assume lossless coupling between the rings as well as between the rings and waveguides, hence $\tau_{a,b}^2 + \kappa_{a,b}^2 = 1$.

The transfer functions (Eq. (1), (2)) show that for a given ring geometry, resonant wavelength and coupling coefficients, the power at D and T port are strongly dependent on the refractive index and absorption of the ring.

Present device is made to operate near 1300 and 1550 nm, which respectively provide lowest dispersion and lowest attenuation during signal transmission. Since the photon energies corresponding to these wavelengths are much smaller than the bandgap of GaAs, these wavelengths, when launched at the input port, will couple to the ring bypassing T port, and appear at D port without undergoing any absorption provided these wavelengths satisfy the resonant condition. For such a resonant wavelength, T port is OFF while D port is ON, and the switch is thus said to be in ON state (optical ON, electrical OFF).

Upon varying the index or absorption of the ring core through an external bias voltage [23, 24], (optical OFF, electrical ON) the wavelength no longer resonates with the ring. Hence, it becomes possible to switch the resonant wavelength between D and T port during electrical OFF to electrical ON phase (and vice-versa). In electrical ON phase (p-i-n diode in forward bias), electrons from the n-AlGaAs cladding and holes from the p-AlGaAs cladding are injected inside the intrinsic ring core. Due to the fact that these carriers are injected via a forward bias, the refractive index of the ring core decreases [25]. The resonant condition is no longer satisfied (i.e, $m\lambda_R \neq 2\pi Rn$ since n decreases due to carrier injection), thereby forcing the resonant signal to switch from the D port and appear at the T port. This makes T port ON and D port OFF for the resonant wavelength, and the switch is said to be in optical OFF state.

In subsequent analyses, it will be shown that the amount of switching depends on the achievable RI change which in turn depends on the applied bias and therefore on injected carrier density.

3. Theoretical model for calculating the index change and micro-ring operation

3.1. Calculation of carrier density for a given bias

To determine the amount of light that can be switched between the two ports of the microring resonator switch, we first need to calculate the number of carriers (electrons and holes) that are injected inside the intrinsic core region of the ring for a given bias. In a semiconductor under steady state, the total current density results from the drift and diffusion of electrons and holes, and is given by [26]

$$\begin{aligned} J_n &= q(\mu_n n F + D_n \nabla n) \\ J_p &= q(\mu_p p F + D_p \nabla p) \end{aligned} \quad (3)$$

where μ_n, and μ_p are the mobilities, D_n and D_n are the diffusion co-efficients, of electron and hole, respectively. The rate of change of carrier concentration of electron and hole due to an applied bias leads to spatial change in current flow, and after accounting for the generation (G) and recombination (R), the rate of change of carrier concentration is represented by the well-known continuity equations

$$\begin{aligned} q\frac{\partial n}{\partial t} &= \nabla \cdot J_n - q(R-G) \\ q\frac{\partial p}{\partial t} &= -\nabla \cdot J_p - q(R-G) \end{aligned} \quad (4)$$

The electric field itself is affected by the charge distribution which includes fixed charges (dopants (p_D, n_A)) and mobile charge carriers (n, p). This electric field is given by Poisson's

#157025 - $15.00 USD Received 25 Oct 2011; revised 8 Apr 2012; accepted 12 Apr 2012; published 26 Jun 2012
(C) 2012 OSA

equation

$$\nabla \cdot F = \frac{q}{\varepsilon}(p - n + p_D - n_A) \quad (5)$$

Equations (3), (4) along with Poisson's equation are self-consistently solved [28, 29] with appropriate boundary conditions at the contacts for the p-i-n structure incorporated inside the microrings. This helps to evaluate the number of electrons and holes that are injected inside the ring core region for a given bias at the contacts.

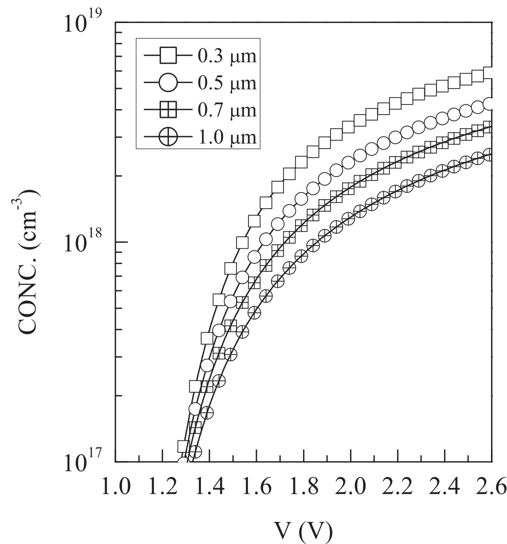

Fig. 2. Injected carrier density inside the p-i-n micro-ring core with applied bias for different i-GaAs core thicknesses 'd' (τ=300ps).

Figure 2 shows the carrier concentration inside the microring core region as a function of applied bias for varying core thicknesses. We have calculated the number of carriers that are injected inside the core for a fixed p-type and n-type doping density of 2×10^{18} cm^{-3}, and Al composition x = 0.3 for both p and n regions. As expected, carrier density increaces with reduction in core thickness.

3.2. Calculation of index change for a given carrier density

Having calculated the number of carriers that are injected inside the ring core as a function of bias, our next task is to determine the RI change of the core due to these injected carriers [31]. The injected carriers alter the RI through three mechanisms such as (i) band gap shrinkage (BGS), (ii) band filling (BF), and (iii) free carrier absorption (FCA). In the following, we will outline the procedure for calculating the index change of the ring core as a function of injected carrier density originating from the above three effects. This is done by first calculating the corresponding absorption change due to injected carriers. The carrier density was obtained by solving the electron and hole transport equations as described in Section 3.1. Any change in the absorption of the material results in a change in the RI, which is obtained by applying Kramers-Kronig integration. This refractive index change will be the one which determines the amount of switching.

#157025 - $15.00 USD Received 25 Oct 2011; revised 8 Apr 2012; accepted 12 Apr 2012; published 26 Jun 2012
(C) 2012 OSA

3.2.1. Index change due to BGS and BF effects

Under carrier injection inside the core region, electrons will be occupying the bottom of the conduction band, while holes will be occupying the top of the valence band. For certain carrier concentration above the critical carrier density, the wave function of the injected carriers will begin to interact with one another. This carrier interaction leads to lowering the conduction band edge, while the top of the valence band edge moves up. The net effect is, therefore, a decrease in the bandgap of the core material. The magnitude of the reduction in bandgap energy is modeled as [32]

$$\Delta E_g(\chi) = \left(\frac{\kappa}{\varepsilon_s}\right)\left(\frac{\chi}{\chi_{cr}} - 1\right)^{1/3} \tag{6}$$

For carrier densities (χ) smaller than the critical carrier density (χ_{cr}), the bandgap reduction is negligible, and hence Eq. (6) assumes the value of zero. Here κ is a constant, and ε_s is the relative dielectric permittivity of the microring material. The change in the absorption of the microring core material due to BGS is then the change in material absorption coefficients when carriers are injected.

Also, the carrier injection induced by the forward bias causes the lower energy states of conduction band of the ring core material to be filled with electrons. When this happens, the absorption of the core material decreases. This phenomenon is termed as Band filling [33]. Note that, while calculating the band filling effect, the change in band gap due to band shrinkage must also be included. It is assumed that optical absorption of the core material follows the square root law [34]. Therefore, the change in the optical absorption of the core material due to band filling with band gap shrinkage included is represented as

$$\begin{aligned}\Delta\alpha_{BF+BGS} &= \frac{C_{hh}}{E}\left(f_v(E_{vh}) - f_c(E_{ch})\right) \times \sqrt{E - E_g'} + \frac{C_{lh}}{E}\left(f_v(E_{vl}) - f_c(E_{cl})\right) \times \sqrt{E - E_g'} \\ &- \left[\frac{C_{hh}}{E}\sqrt{E - E_g} + \frac{C_{lh}}{E}\sqrt{E - E_g}\right]\end{aligned} \tag{7}$$

where the terms in the square bracket give the absorption of the unperturbed ring core (i.e. with no bias). The constants C_{hh}, C_{lh} are taken from [32] with a multiplicative correction term of $\sqrt{\hbar}$. Here, f_v and f_c are the Fermi probability functions obtained after considering the carrier-dependent quasi-Fermi levels and reduced bandgap (E_g') obtained from Eq. (6). The model also takes care of the degeneracy of the valence band. After obtaining the absorption change due to the combination of the BF and BGS effects, the corresponding RI change (Δn_{BF+BGS}) is obtained using the Kramers-Kronig integration given by [5]

$$\Delta n_{BF+BGS} = \frac{c\hbar}{\pi}\text{PV}\left(\int_0^\infty \frac{\Delta\alpha_{BF+BGS}}{\bar{E}^2 - E^2} d\bar{E}\right) \tag{8}$$

where c is the speed of light, $E = \hbar\omega$ is the photon energy, $\bar{E}$ is the variable of integration, and 'PV' represents the Cauchy principal value of the integral. All calculations were done in the wavelength domain by utilizing the relationship $E = hc/\lambda$. The integral was numerically computed using a wavelength interval spacing of 0.01 nm.

3.2.2. Index change due to FCA effect

Free-carrier absorption originates due to the absorption of photons by the free carriers (electrons or holes) in the conduction or valence band of the core material [35]. The RI change of the ring core due to FCA effect is given by

#157025 - $15.00 USD Received 25 Oct 2011; revised 8 Apr 2012; accepted 12 Apr 2012; published 26 Jun 2012
(C) 2012 OSA

$$\Delta n_{FCA} = -\frac{6.9\times10^{-22}}{nE^2}\left[\frac{N}{m_e} + P\left(\frac{m_{hh}^{1/2}+m_{lh}^{1/2}}{m_{hh}^{3/2}+m_{lh}^{3/2}}\right)\right] \quad (9)$$

Here N and P represents the number of electrons and holes that are injected inside the ring core, respectively, and m_e, m_{lh} and m_{hh} are the effective masses of electron, light-hole and heavy-hole of the microring core material, respectively.

3.2.3. Total Index Change

The net RI change of the ring core is the summation of RI changes due to the combined three effects i.e.

$$\Delta n_{Total} = \Delta n_{BF+BGS} + \Delta n_{FCA} \quad (10)$$

This index change is the parameter that ultimately determines the amount of the light that can be switched between the D and T ports.

3.3. Results and discussions on switching of micro-ring resonator p-i-n diode

We will now present the calculated results obtained for the RI change of the ring core for various applied biases (hence injected carrier densities). Figure 3(a) shows the RI change of the ring core due to the combination of BF effect and BGS effect as a function of the operating wavelength for various injected carrier densities. It is obvious from Eq. (7) that for injected carrier densities smaller than the critical carrier density, the BGS effect is absent, and hence, the RI change is mainly due to the BF effect. We also notice that the RI change due to carrier injection is negative for photon wavelengths longer than the wavelength corresponding to the band edge. As the injected carrier density just crosses the critical carrier density, the contribution due to the BGS effect increases, leading to a positive net index change induced by the combination of the BGS and BF effects. For further increase in the injected carrier density, negative RI change is observed, due to the fact that the BF effect is partially cancelled by the positive RI change caused by the BGS effect. However, the net index change due to the combination of BF and BGS effects is still negative since BF effect always dominates over BGS effect. We also note that the largest index change happens near the bandedge when both the BGS and BF effects are present, and that the magnitude of RI change falls off rapidly as the signal wavelength exceeds the bandedge wavelength.

Figure 3(b) depicts the RI change as a function of wavelength due to the free-carrier absorption effect, for different applied bias. It is noticed that, in contrast to the BGS and BF effects, the magnitude of the RI change due to the FCA effect increases as the signal wavelength exceeds the band edge (i.e, for increasing wavelengths) due to the λ^2 dependance of Δn_{FCA}. It is also noticed that the RI change due to the FCA effect is always negative.

Figure 4 plots the overall index change (i.e, $\Delta n_{BF+BGS} + \Delta n_{FCA}$) as a function of operating wavelength for various bias points, which inturn corresponds to various carrier densities. Beyond the bandedge wavelength, the overall RI change is always negative. Also, the index change is maximum near the bandedge of ring core (GaAs), which occurs at around 870 nm, while it falls off at higher wavelengths. However, it is interesting to note that even for wavelengths far from the bandedge wavelength (i.e., for longer wavelengths) still a significant RI change occurs due to injected carriers which can be used for switching. Also, the magnitude of the RI change increases with increasing carrier density, which implies, for an operating wavelength far from the bandedge wavelength, a large overall RI change is still achievable if the carrier injection is increased (via an increased bias voltage). This RI change induced in GaAs material is large enough that it enables the proposed microring resonator switch to be used over the long wavelength window of optical telecommunications, which is well beyond the conventional 870 nm

#157025 - $15.00 USD Received 25 Oct 2011; revised 8 Apr 2012; accepted 12 Apr 2012; published 26 Jun 2012
(C) 2012 OSA

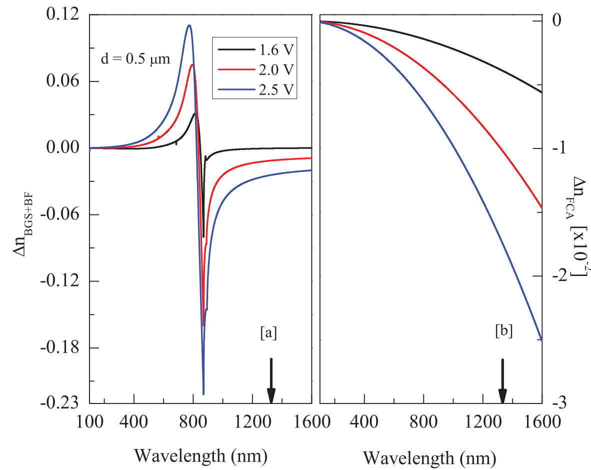

Fig. 3. (a) Refractive index change (Δn_{BGS+BF}) of p-$Al_{0.3}Ga_{0.7}As$/i-GaAs/n-$Al_{0.3}Ga_{0.7}As$ p-i-n ring core due to combined BGS and BF effects for various applied bias, which is estimated as a function of operating wavelength. Arrow on the X-axis indicates resonant wavelength, and, (b) refractive index change (Δn_{FCA}) of the identical device due to FCA effect for various applied bias, which is estimated as a function of operating wavelength. Like before, arrow on the X-axis indicates resonant wavelength.

bandedge wavelength of GaAs. It is to be noted that the RI change of the microring core decreases for increased carrier density which means that the resonant wavelength of the microring undergoes a blue shift. In contrast, carrier depletion of the microring core results in an increase of the ring core RI, thereby red shifting the resonant wavelength.

For a given ring radius, several wavelengths can resonate within the ring. In our design, we fix the ring radius to be 5 μm, and thus 1560.16 nm and 1305.28 nm are the two resonant wavelengths of our choice which happened to be near the telecom wavelengths. Hence, we will now examine in detail the RI change as well as the switching characteristics of the ring resonator switch for the resonant wavelengths 1560.16 nm and 1305.28 nm. For switching calculations, κ_a was taken to be 0.35, and $\kappa_b = 0.5 \times \kappa_a^2$ as per [16] in order to obtain a maximally flat response at the Drop and Transmit port of the ring resonator switch. We also considered the wavelength dependent RI of GaAs as per [26].

Figure 5(a) and 5(b) show the RI change of the microring core as a function of injected carrier densities at selected resonant wavelengths. The corresponding applied bias that achieved the required carrier density can be inferred from Fig. 2. It is found that for an injected carrier density of up to $\sim 10^{17}\text{cm}^{-3}$, the RI change of the core material is quite small to cause any appreciable effect on the light propagation. Thus until the injected carrier density reaches the critical carrier density, the switch may be treated as insensitive to carrier injection, and applied bias. However, a further increase in the bias (and the injected carrier density) causes the RI of the core material to reduce significantly. For an injected carrier density of 4×10^{18} cm^{-3}, a significant RI change of -0.05 is attained. It is also noticed from Fig. 5 that the RI change increases with increasing the carrier density as well as the forward bias voltage, as expected.

Having calculated the RI changes both as functions of the carrier density and the applied bias for the wavelengths of interest, we can now predict the switching performance of the ring resonator switch by utilizing Eqs. (1), (2) along with the computed RI values as shown

#157025 - $15.00 USD Received 25 Oct 2011; revised 8 Apr 2012; accepted 12 Apr 2012; published 26 Jun 2012
(C) 2012 OSA

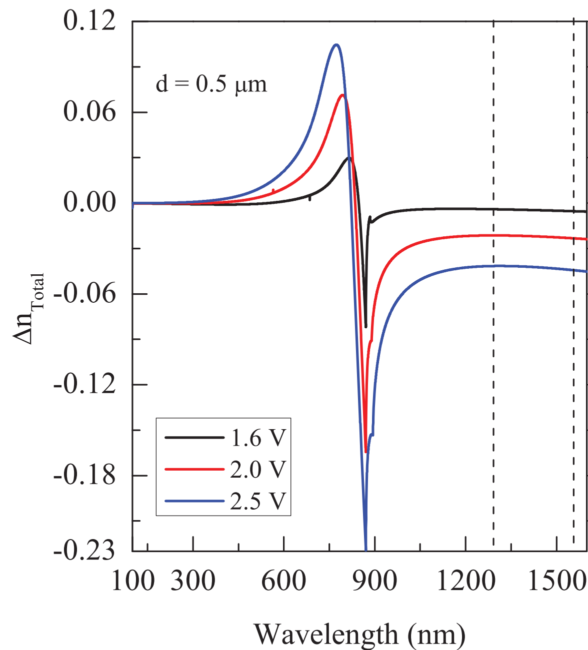

Fig. 4. Total refractive index change as a function of operating wavelength due to the combination of the BGS, BF and FCA effects for various applied bias. It is seen that for operating wavelengths far from bandedge wavelength, significant index change occurs whose magnitude is more than adequate to realise switching in ring resonator. The black dotted lines show the wavelengths we aim to switch.

in Fig. 5. An input signal of wavelength λ_R = 1560.16 nm couples to the ring and appears at the D port without any absorption since the photon energy corresponding to this resonant wavelength (∼0.8 eV) is much smaller than the ring core bandgap (1.424 eV). The applied bias is set to zero; hence there is no carrier injection into the ring core. However, due to the spilling of electrons and holes from the p and n doped cladding regions, a small number of carriers are usually present at the intrinsic core region [36]. Our calculations confirm that, for the proposed switch structure, the carrier density originating from the spilling is as small as $10^6 cm^{-3}$, making it too small to cause any appreciable effect on the propagating optical signal through the microring resonator. Thus, a 1560.16 nm optical signal launched into the input port will appear at the D port without any attenuation (i.e. the D port of the switch is in the ON state for λ_R = 1560.16 nm).

Figure 6(a) and 6(b) show the output spectra of the T and D ports for two different bias voltages and resonant wavelengths of 1305.28 and 1560.16 nm. It is obvious that for λ_R = 1560.16 nm and, V=0 V, the normalised optical intensities at the T and D ports are -25 dB and 0 dB, respectively, resulting in an interport isolation of 25 dB. This implies that D port is ON and T port is OFF at the resonant wavelength. Note also that, in this case, the RI change is zero since no carriers are injected. Upon forward biasing, carriers are electrically injected from the p and n side into the ring core region, and the carrier density at the core increases significantly. It was found that at a forward bias of 2 V, the injected carrier density in the ring core is about 2.33×10^{18} cm^{-3}, resulting in a decrease in the refractive index of the core by 0.02 (due to the three effects described in Sections 3.2.1 and 3.2.2), thereby switching λ_R from the D port to the

#157025 - $15.00 USD Received 25 Oct 2011; revised 8 Apr 2012; accepted 12 Apr 2012; published 26 Jun 2012
(C) 2012 OSA

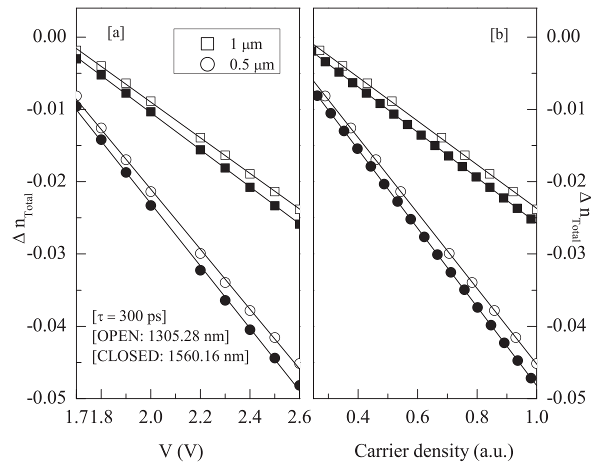

Fig. 5. (a): Total refractive index change (Δn_{Total}) due to the combination of BGS, BF and FCA effects, with applied bias for p-$Al_{0.3}Ga_{0.7}As$/i-GaAs/n-$Al_{0.3}Ga_{0.7}As$ p-i-n diode of 1 μm and 0.5 μm intrinsic-GaAs region thicknesses (τ = 300 ps). Δn_{Total} is estimated for 1305.28 and 1560.16 nm input wavelengths, (b) Total refractive index change (Δn_{Total}) with electrically injected normalized carrier density into 1 μm and 0.5 μm intrinsic-GaAs layer (τ = 300 ps), which is individually estimated with 1305.28 and 1560.16 nm input wavelengths. As seen from Fig. 2, for fixed bias, injected carrier density is smaller in thicker core, and smaller index change is thus expected for 1 μm core thickness.

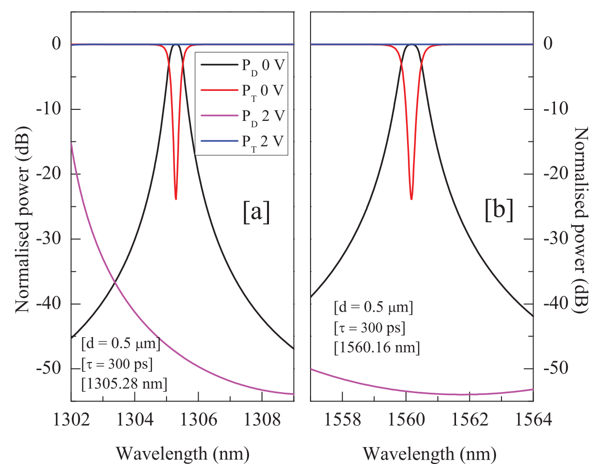

Fig. 6. (a)Normalised power spectra for λ_R = 1305.28 nm, sampled at T(RED), D(BLACK) ports and, T(BLUE), D(MAGENTA) ports for 0 V and 2 V applied biases respectively, (b)Normalized power spectra for λ_R = 1560.16 nm, sampled at T(RED), D(BLACK) ports and, T(BLUE), D(MAGENTA) ports for 0 V and 2 V applied biases respectively.

#157025 - $15.00 USD Received 25 Oct 2011; revised 8 Apr 2012; accepted 12 Apr 2012; published 26 Jun 2012
(C) 2012 OSA

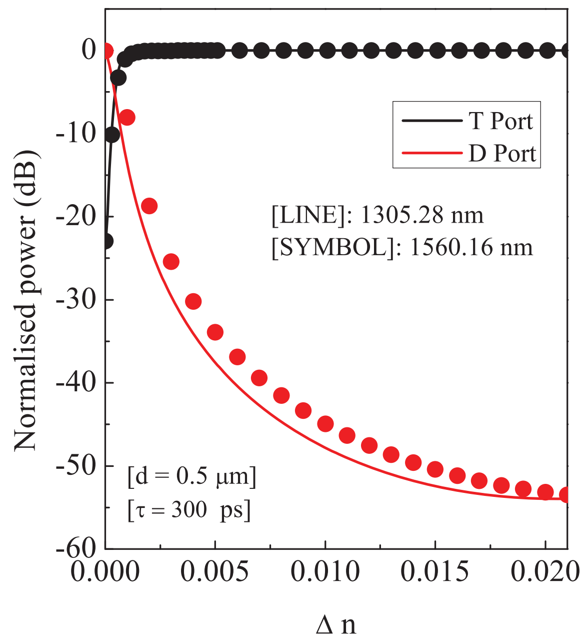

Fig. 7. Normalised output power level at the T (black) and D (red) ports versus the magnitude of RI change for two different resonant wavelengths (1305.28 nm, 1560.16 nm). Note that the RI change is negative.

T port.

Figure 7 shows the output power levels at the T and D ports versus the index change (due to biasing) for operation over the 1550 nm and 1300 nm bands. It is noticed that as the index change increases the inter-port isolation increases. For an interport isolation of 30 dB, the index change is around 0.004, which corresponds to a bias voltage of less than 1.5 volts.

In summary, Figs. 6 and 7 demonstrate the principle of the proposed GaAs-based microring resonator switch and its potential for switching signals over the 1300 nm and 1550 nm telecommunication windows. Note that III-V optical switches operating at telecom wavelengths are built on InP substrates with InGaAsP/InP, InAlAs/InGaAs quantum wells or bulk material since these materials provide bandgaps close to the photon energies of telecom wavelengths. However, such InP based optical telecommunication switches have several drawbacks, including (i) high-cost due to scarcity of Indium, (ii) immature processing technology in comparison to the GaAs technology (iii) high insertion loss, (iv) small wafer sizes and fragility, and (v) presence of inflammable and toxic Phosphorous material in epitaxial growth system. To circumvent the high-cost and fragility of InP wafers, efforts have been directed to realise long wavelength switches and modulators by growing “In” based ternary and quaternary materials onto GaAs substrate. Unfortunately, such an approach requires complicated growth techniques [37] due to the lattice mismatch between In based materials and GaAs substrate. Also, the operating wavelength of the device is critically decided by the Indium composition. Achieving long wavelength operation in this case is somewhat difficult, since increasing In composition increases the lattice mismatch [38, 39] thereby degrading the device performance.

On the other hand, the proposed GaAs microring resonator switch completely eliminates not only the usage of Indium and Phosphorous materials, but also avoids the formation of quantum

#157025 - $15.00 USD Received 25 Oct 2011; revised 8 Apr 2012; accepted 12 Apr 2012; published 26 Jun 2012
(C) 2012 OSA

wells. As a result, the proposed switch is highly cost effective. More importantly, the device enables the switching of *any long wavelength signals* as long as they are in resonance with the microring; thereby breaking the interdependence between the choice of material composition and operating wavelength. This offers a tremendous amount of flexibility to choose the operating wavelength of the switch.

4. Electrical performance of p-i-n micro-ring resonator switch

To assess electrical switching performance of the proposed micro-ring resonator p-i-n device, we have individually estimated power and delay during turn-on and turn-off phases through solving closed form p-i-n diode equations [27]. Average carrier density (n_a) in (intrinsic) i-GaAs core of micro-ring is extracted following Fig. 2.

For a p-i-n diode having half intrinsic layer thickness d and, carrier recombination lifetime τ, the maximum current density (J_T) is given as,

$$J_T = n_a \left(\frac{2qd}{\tau} \right) \tag{11}$$

During the turn-on phase of the switch, the time dependence of J_T can be expressed as,

$$J(t) = \begin{cases} \left(\frac{J_T}{\tau}\right) \times t, & 0 \le t \le \tau \\ J_T, & t > \tau \end{cases} \tag{12}$$

It is evident from Eq. (12) that, for lower τ, recombination rate is faster, so is the ramp rate $\frac{J_T}{\tau}$ before attaining towards the steady state current density. Additionally, during turn-on process, the space-time dependence of the injected electron density $n(x,t)$ is given by,

$$n(x,t) = A(t) \exp\left(-\frac{x}{\sqrt{4D_n t}} \right) + n_i \tag{13}$$

in which

$$A(t) = \frac{\left(\frac{J_T}{\tau}\right) t^{3/2}}{q\sqrt{D_n}} \tag{14}$$

Following convention, D_n is the electron diffusion coefficient and n_i is the intrinsic carrier density in i-GaAs micro-ring core region. Note that for high-level injection $n(x,t) = p(x,t)$, therefore, space-time evolution of one type of carrier (electron) is sufficient to understand electrical performance of the device.

Figure 8 shows the temporal evolution of $n(x,t)$ during turn-on phase of micro-ring p-i-n diode. Modulation length (X_M) is defined as the distance at which, $n(x,t)$ attains the modulation concentration N_M and is expressed as,

$$X_M = \sqrt{4D_n t} \log \left[\frac{A(t)}{N_M - n_i} \right] \tag{15}$$

Note that N_M is taken as the $\frac{1}{e}$ times the maximum carrier density for each time slice of $n(x,t)$. It is evident from Fig. 8 that, $n(x,t)$ grows with time along the i-GaAs/n-$Al_{0.3}Ga_{0.7}As$ interface (x = 0), hence X_M moves deep inside i-GaAs core, which soon crosses the carrier diffusion length in few ps of initial transient. For electron lifetime of 300 ps, diffusion length is estimated as $\sim$0.77 μm.

#157025 - $15.00 USD Received 25 Oct 2011; revised 8 Apr 2012; accepted 12 Apr 2012; published 26 Jun 2012
(C) 2012 OSA

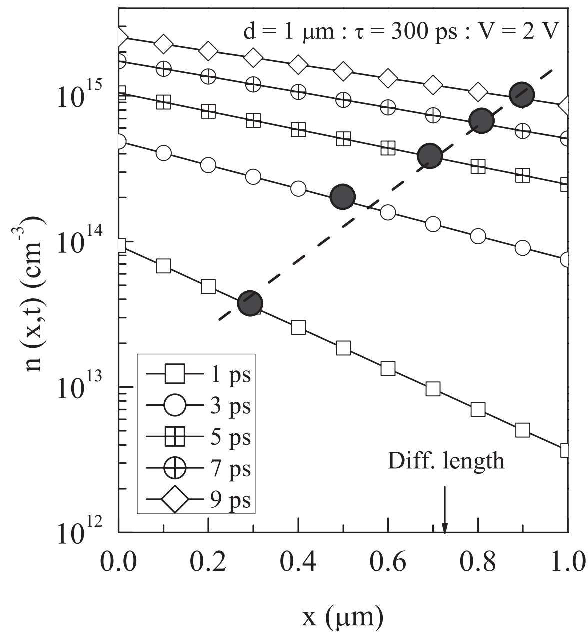

Fig. 8. Temporal evolution of n(x,t) at the initial switching phase (turn-on) for p-$Al_{0.3}Ga_{0.7}As$/i-GaAs/n-$Al_{0.3}Ga_{0.7}As$ p-i-n diode of 1 μm intrinsic-GaAs region thickness. Locus of modulation length (X_M) (see text for definition) is indicated by dashed line.

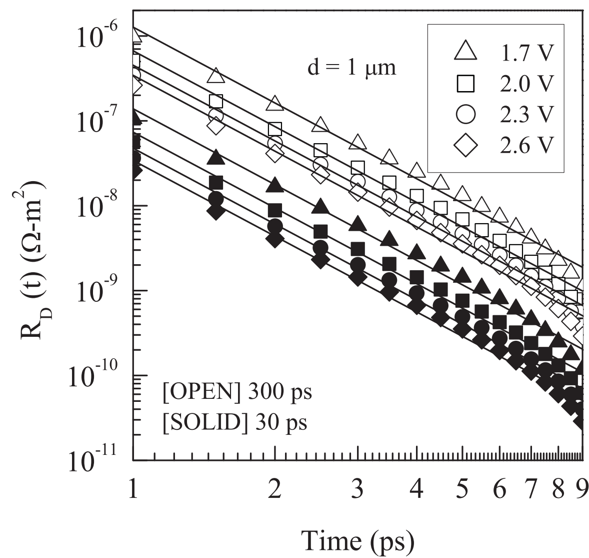

Fig. 9. Time evolution of intrinsic-region (drift space) resistance for p-$Al_{0.3}Ga_{0.7}As$/i-GaAs/n-$Al_{0.3}Ga_{0.7}As$ p-i-n diode of 1 μm i-GaAs region thickness, with individual applied bias at the initial switching phase (τ=300 ps and, τ=30 ps). Lines are guide to the eye.

#157025 - $15.00 USD Received 25 Oct 2011; revised 8 Apr 2012; accepted 12 Apr 2012; published 26 Jun 2012
(C) 2012 OSA

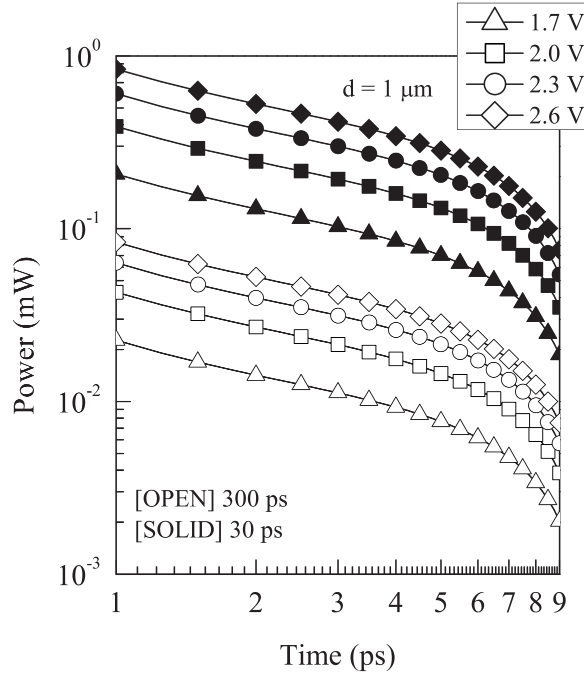

Fig. 10. Time evolution of power (in un-modulated drift space) for p-$Al_{0.3}Ga_{0.7}As$/i-GaAs/n-$Al_{0.3}Ga_{0.7}As$ p-i-n diode having 1 μm i-GaAs region thickness, with individual applied bias at the initial switching phase (τ=300 ps and, τ=30 ps).

Figure 9 shows the temporal evolution of drift-region (i-GaAs) resistance with applied bias, for two different carrier lifetimes. Time dependent drift-region resistance $R_D(t)$ is expressed as follows,

$$R_D(t) = \int_{X_M}^{d} \frac{dx}{q\mu_n n(x,t)} \tag{16}$$

Here, μ_n is the electron mobility inside i-GaAs which is taken as constant for sparse carrier distribution beyond X_M. As seen from Fig. 8 for smaller time slice, injected carrier density inside drift region reduces drastically, thereby increases drift region resistance. In contrast to that, in few ps of initial phase of turn-on transient, as the growth front of $n(x,t)$ progresses deep inside i-GaAs, X_M rapidly crosses diffusion length, therefore for higher conductivity modulation $R_D(t)$ reduces with time. In fact on the other hand, if the carrier lifetime reduces by ten-fold (30 ps), for higher current ramp rate (see Eq. (12)), $R_D(t)$ reduces more rapidly as compared to that of 300 ps case.

Figure 10 shows the time evolution of power $P(t)$ inside un-modulated i-GaAs during turn-on transient, which is estimated using following expression,

$$P(t) = J^2(t) \times R_D(t) \times \pi R^2 \tag{17}$$

where R is the radius of the micro-ring.

As illustrated before, for conductivity modulation with time, $R_D(t)$ reduces in few ps of turn-on phase and hence dissipation, which is observed in Fig. 10 as well. Moreover, for high ramp rate, power dissipation is more if electron lifetime inside i-GaAs core reduces by ten-fold (30

#157025 - $15.00 USD Received 25 Oct 2011; revised 8 Apr 2012; accepted 12 Apr 2012; published 26 Jun 2012
(C) 2012 OSA

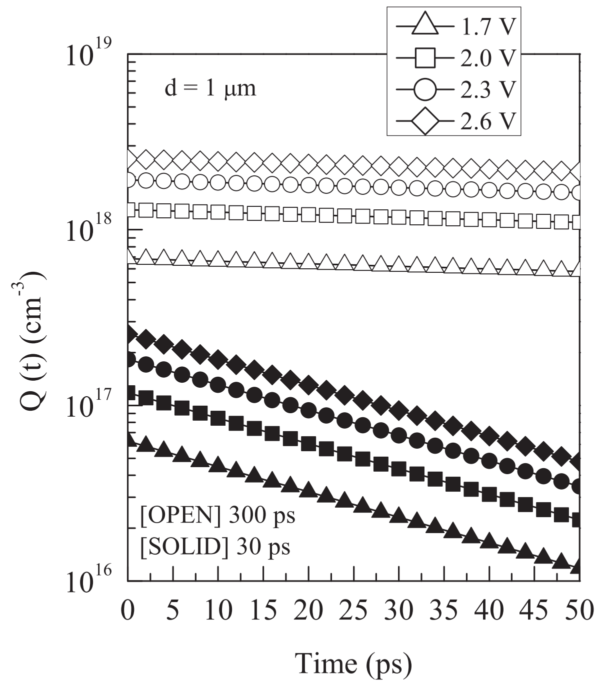

Fig. 11. Decay of steady state stored charge density with time during turn-off phase of p-$Al_{0.3}Ga_{0.7}As$/i-GaAs/n-$Al_{0.3}Ga_{0.7}As$ p-i-n diode of 1 μm i-GaAs region thickness (τ=300 ps and, τ=30 ps).

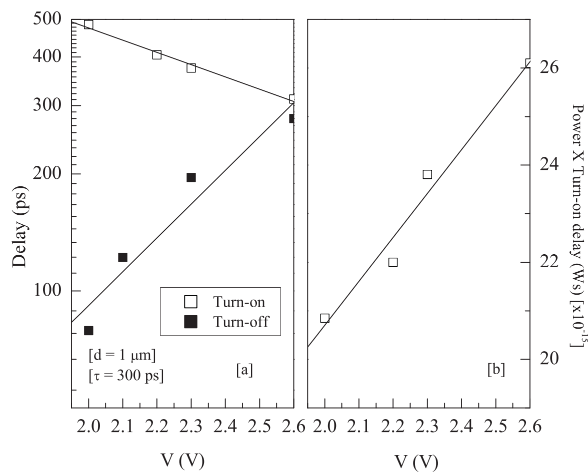

Fig. 12. Turn-on and turn-off delays of p-$Al_{0.3}Ga_{0.7}As$/i-GaAs/n-$Al_{0.3}Ga_{0.7}As$ p-i-n diode of 1 μm i-GaAs layer thickness. (b) Power-delay product of identical diode during turn-on phase (τ = 300 ps).

#157025 - $15.00 USD Received 25 Oct 2011; revised 8 Apr 2012; accepted 12 Apr 2012; published 26 Jun 2012
(C) 2012 OSA

ps). Nevertheless, the power dissipation is an important metric during initial switching phase, which becomes saturated once the p-i-n diode enters into the steady state.

Figure 11 shows the decay of steady state charge density inside i-GaAs layer during turn-off phase of the micro-ring resonator switch. Charge decay $Q(t)$ is modeled through,

$$\frac{dQ}{dt} = -\frac{Q}{\tau} \tag{18}$$

As expected, decay rate is faster for ten-fold reduction in carrier lifetime (30 ps), which is therefore desirable for faster turn-off response. However, for higher ramp rate and for smaller carrier life-time, dissipation peak is higher during turn-on phase, which we have discussed before.

Figure 12(a) shows the turn-on delay of p-i-n micro-ring device, which is defined as the time required to achieve 1% total refractive index change (threshold carrier density 1.3×10^{18} cm^{-3}), so as to block the light transmission between T and D ports. As expected, turn-on delay reduces with increase in applied bias for faster-ramp rate. In contrast, turn-off delay is defined as the time needed to reduce steady state carrier density below 1.3×10^{18} cm^{-3} (threshold), so as to prevent appreciable refractive index change in i-GaAs core material. Turn-off delay increases with bias, for higher stored charge density. Figure 12(b) shows the power-delay product during turn-on phase of 1 μm thick i-GaAs device. Although is extremely small, however, the power-delay product increases with bias for higher power dissipation, which indeed requires to be minimized without affecting device operation.

5. Conclusions

We have proposed and analyzed GaAs double microring resonator optical switch using bias assisted carrier injection as the refractive index modulating mechanism. We have shown that optical switching can be achieved by electrically injecting carriers into the microrings through application of forward bias voltage thereby changing the refractive index of the core material. Detail results have shown that the switching of optical signals over the 1300 nm and 1550 nm windows is feasible because significant refractive index change can be obtained through the application of bias voltage as small as 2 V. More importantly, we found that the proposed GaAs based optical switch can successfully switch long wavelength signals (1550 nm and 1300 nm) by neither requiring InP substrates nor by growing ternary and quaternary Indium based materials on GaAs substrate. Moreover, besides optical switching, we have thoroughly evaluated electrical performance of the proposed device considering power-delay figures. The proposed switch has a smaller footprint when compared to MZI or DC based switch, thereby making it attractive for large scale optoelectronic integration, optical communication and optical interconnects.

Acknowledgments

This work was partially supported by “Systems biology infrastructure establishment grant”, by World Class University (WCU) program at GIST through a grant provided by MEST of Korea (R31-20008-000-10026-0) and by “Photonics2020” research project through a grant provided by the GIST in 2012. Technical discussions and suggestions from Seung-Yong Nam and Dr. Sung-Jun Jang, School of Information and Communications are gratefully acknowledged. S. R would like to thank RS group members for their constant encouragement.

#157025 - $15.00 USD Received 25 Oct 2011; revised 8 Apr 2012; accepted 12 Apr 2012; published 26 Jun 2012
(C) 2012 OSA